PHYSICAL REVIEW B **91**, 064103 (2015)

Point defect stability in a semicoherent metallic interface

C. González,[1,*] R. Iglesias,[1] and M. J. Demkowicz[2]
[1]*Departamento de Física, Universidad de Oviedo, 33007 Oviedo, Spain*
[2]*Department of Materials Science and Engineering, Massachusetts Institute of Technology (MIT), Cambridge, Massachusetts 02139, USA*
(Received 6 September 2014; revised manuscript received 20 January 2015; published 11 February 2015)

We present a comprehensive density functional theory (DFT) -based study of different aspects of one vacancy and He impurity atom behavior at semicoherent interfaces between the low-solubility transition metals Cu and Nb. Such interfaces have not been previously modeled using DFT. A thorough analysis of the stability and mobility of the two types of defects at the interfaces and neighboring internal layers has been performed and the results have been compared to the equivalent cases in the pure metallic matrices. The different behavior of fcc and bcc metals on both sides of the interface has been specifically assessed. The modeling effort undertaken is the first attempt to study the stability and defect energetics of noncoherent Cu/Nb interfaces from first principles, in order to assess their potential use in radiation-resistant materials.

DOI: 10.1103/PhysRevB.91.064103 PACS number(s): 68.35.Ct, 68.35.Dv, 68.35.Fx

I. INTRODUCTION

Nuclear fusion energy has been long foreseen as an environmentally clean and practically infinite energy source that could fulfill the goals of sustainable and affordable energy production in the future. The high energy neutrons produced can induce a large number of defects such as vacancies and interstitial clusters where He/H atoms can be accumulated forming bubbles. These defects can lead to volume swelling and blistering that decreases the stability of reactor components reducing their service life [1]. For that reason, a deeper understanding of materials behavior in extreme environments is essential to mitigate all radiation-induced defects improving the reliability, lifetime, and integrity of structural materials in advanced reactors.

Materials containing a high concentration of interfaces promise to offer high resistance to radiation damage accumulation [2]. Enhanced radiation performance is due to grain boundaries and interfaces between incoherent metallic nanosized multilayers that act as effective sinks for defect recombination at intersections between misfit dislocations [3]. Experimentally, multilayered Cu/Nb composites with nanodimensional interlayer spacing exhibit excellent resistance to irradiation-induced structural changes [4,5]. The detrimental effects in irradiated materials due to the presence of He bubbles can be controlled via efficient tailoring of the multilayered composite morphology [6].

It is well known that first-principles calculations, in particular density functional theory (DFT), provide a wealth of highly valuable information on materials properties at 0 K. It is by no means trivial to establish meaningful links to the properties at larger time and length scales and finite temperatures. DFT techniques are the first crucial step to create an energy and force database that provides a solid foundation for subsequent molecular dynamics (MD) and kinetic Monte Carlo (kMC) simulations lying at an upper level of what has become commonly known as a multiscale modeling approach [7]. Following this idea, a new DFT-based embedded atom method interatomic Cu-Nb-He potential has been developed [8] and subsequently used in MD simulations to obtain formation, binding, and migration energies of helium clusters in Cu-Nb that in turn are input for kMC codes [9]. Subsequently, stable and efficient storage of He bubbles at interfaces has been theoretically proposed in the Cu/Nb system [10]. Recently, another way of efficiently simulating certain properties of interfaces has been presented by using reduced order models based on elasticity theory [11].

The study of noncoherent interfaces is intrinsically difficult with DFT because it can only deal with relatively small models. This fact has limited in practice DFT simulations to coherent interfaces, which are strained so that the neighboring crystals have perfect, atom-to-atom matching. These kinds of calculations have been performed before for different coherent grain boundaries [12–15]. In the first example, Xiao and Geng [12] studied the accumulation of H atoms in the $\Sigma 3(111)$ tilt grain boundary of W introducing a mirror symmetry in the middle of the slab. In a similar way, Korner *et al.* studied ZnO grain boundaries and Huber *et al.* [14] analyzed the binding energy of different metals in the $\Sigma 7$ grain boundary in Mg. Finally, Hunter and Beyerlein [15] studied the size and evolution of stacking faults formed at grain boundaries in different fcc metals (Al, Cu, Ni, Au, Pd, and Ag).

However, the properties of most noncoherent interfaces, such as the Cu/Nb interface, are primarily due to the intrinsic defects that arise from imperfect matching of the atomic structures across the interface. Accounting for this inherent, internal structure is a computational challenge that, in the past, has consigned the study of noncoherent interfaces to the realm of classical potential simulations or to hybrid approaches that combine first-principles with continuum elasticity models [16]. Only recently, metallic vacancies and self-interstitials has been studied by DFT using a small supercell of a semicoherent Cu/Nb interface [17].

In this paper, we present a DFT-based energetic analysis of monovacancy type and He impurity point defects at a Cu/Nb semicoherent interface and neighboring layers. The results show the preferential trapping of He at the so-called misfit dislocation intersections (MDIs) and suggest that barriers to He migration within the interface are high. A similar behavior has been found for a monovacancy in both Cu and Nb metals. Typically, helium atoms in bulk metals tend to be

*cesar.gonzalez.pascual@gmail.com

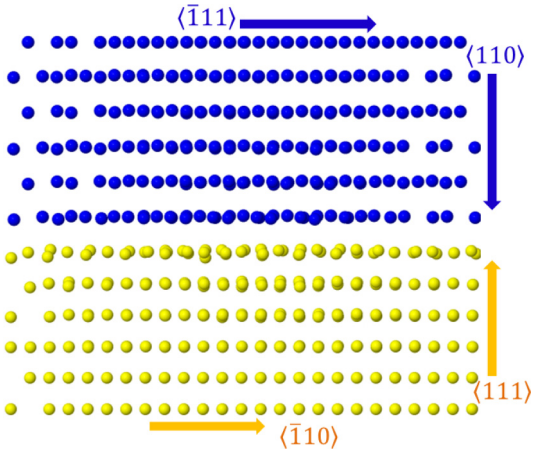

FIG. 1. (Color online) Lateral view of the Cu/Nb interface. Yellow/blue spheres represent Cu/Nb atoms respectively.

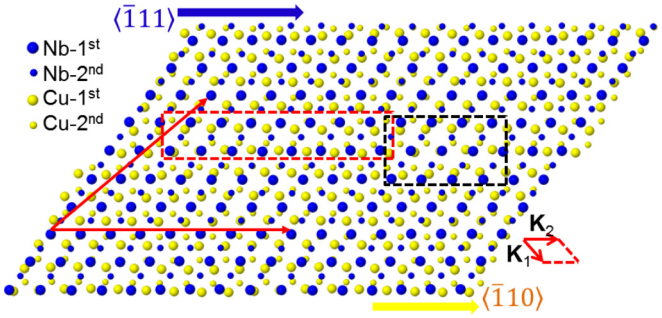

FIG. 2. (Color online) Frontal view of the Cu/Nb interface. Yellow/blue spheres represent Cu/Nb atoms respectively, being the bigger ones at the interface. The MDI area is outlined by a dark square and is expanded in Fig. 3. The red rectangle corresponds to the area analyzed in Figs. 4 and 5. The superimposed red arrows are the lattice vectors used in the simulation (corresponding to a superficial Cu-9 × 6 cell). The corresponding vectors of the reciprocal lattice as well as of the 2D first Brillouin zone are included in the bottom right side of the figure.

stabilized inside monovacancies rather than in their interstitial positions. According to our energetic analysis, isolated He atoms would also prefer to occupy a metallic vacancy immediately adjacent to the interface instead of the main Cu/Nb interface.

II. METHOD OF CALCULATION

First-principles calculations were performed using the *Vienna ab initio simulation package* (VASP) code [18]. Based on DFT techniques, this plane-wave code uses very efficient pseudopotentials generated with the projector augmented wave (PAW) method [19]. The widely used Perdew-Burke-Ernzerhof parametrization of the generalized gradient approximation has been chosen as the exchange and correlation functional [20]. The lattice parameters of both metals found previously by the authors are 3.63 Å for Cu [21] and 3.316 Å for Nb [22], only 0.5% higher than the experimental evidence [23]. The valence electrons for the different elements used in the calculation are 11 for Cu (ten $3d$ and one $4s$), 11 for Nb (six $4p$, four $4d$, and one $5s$) and two $1s$ valence electrons for He.

Six layers of each of the Cu ⟨111⟩ and Nb ⟨110⟩ surfaces have been built and relaxed separately. As suggested experimentally [4,5], the Cu/Nb interface is formed preferentially in the Kurdjumov-Sachs geometry [24]. Proper simulation under periodic boundary conditions consistent with a DFT-PAW code requires a 9 × 6 (324 Cu atoms) and an 8 × 5 (240 Nb atoms) surface slab, respectively (see the standard lattice vectors in Fig. 2). In order to obtain the best possible fit between both metallic surfaces, the dimensions of the Nb layer have been constrained to those of Cu, leading to an expansion of about 0.5%. Then, the metals are placed together to construct a 12-layer slab (see Fig. 1). Initially, the separation between both surfaces is fixed to that between two Nb ⟨110⟩ bulk planes, namely, 2.33 Å. A vacuum of 10 Å separates the two free surfaces of the slab containing the interface.

Next, the system is fully and self-consistently relaxed, except for the deepest layer of each metal that is kept fixed. In a first step the system is relaxed using only the Γ point, to be finally refined with 9 k points in the two-dimensional (2D) first Brillouin zone (shown in the right part of Fig. 2). Further details about the energy convergence with the k points will be discussed below. The cutoff energy of the plane waves was fixed to 479 eV as recommended in VASP for calculations involving He atoms and the system is relaxed until the forces are smaller than 0.025 eV/Å. As a final step, the distance between the fixed layers is varied until the energy minimum of the most stable interface is found. Additionally, the Nb part of the slab has been allowed to relax in the XY direction (fixing the Z coordinate of the last layer) until the most stable structure was found.

The lateral view of the resulting structure is shown in Fig. 1. Although there is no mixing between the atoms of the first layers, a great reconstruction is observed at the interface. The different layers in both metals present an important structural corrugation, defined as the difference between the larger and smaller Z coordinates of the atoms in each layer. At the interface, the corrugation of the first Cu layer is almost double that of the first Nb layer: 0.58 Å vs 0.26 Å, respectively. For deeper layers, the corrugation decreases quite fast in Cu (0.41 Å and 0.20 Å for the second and third layers, respectively), while for Nb it remains stable (0.25 Å for those two layers). These relatively high corrugations obtained in the defect-free interface motivate the use of at least six layers per metallic slab to capture the strain fields generated at the interface.

Subsequently, the two types of defects (vacancies and He atoms) are in turn placed in the regions close to the interface. The corresponding formation energy of each defect is defined as

$$E_f = E_{\text{tot}} + n_{\text{vac}} E_{\text{metal}} - N_{\text{He}} E_{\text{He}} - E_{\text{Int}}, \qquad (1)$$

where E_{tot} and E_{Int} are the final total energies obtained after the VASP relaxation of a given configuration and the initial relaxed interface, respectively. E_{He} is the energy of an isolated He atom placed inside a large empty simulation box, n_{vac} is the number of vacancies in each metal (only one in what follows), and E_{metal} is the atomic energy of a single Cu or Nb bulk atom. This definition is consistent with others appearing in the literature [25] and with the expression previously used for Cu and Nb bulk values (see, for example, Ref. [21]). The size of the slab

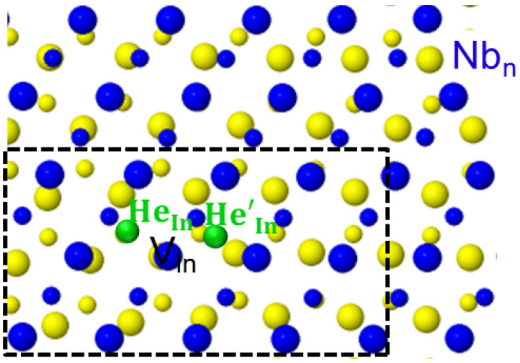

FIG. 3. (Color online) Frontal view of the outlined area inside the black square in Fig. 2 corresponding to the MDI area. He_{In} (He'_{In}) and V_{In} indicate the preferential sites for a He atom and a vacancy, respectively. Nb_n indicates the Nb atom outside of the MDI area analyzed in the text. Yellow/blue spheres represent Cu/Nb atoms respectively, being the bigger ones at the interface.

is large enough to represent one unit cell of the interface misfit dislocation pattern [26]. We use the nudged elastic band (NEB) method to find activation energies for defect migration [27].

III. RESULTS

Once we have created a model of the Cu/Nb interface, the first goal of this study is to find the most stable sites for the three different defects: a He interstitial and a metallic vacancy created either in Cu or in Nb separately. Interestingly, the area where the three types of defects are more stable is the same and corresponds to the zone inside the black square in Fig. 2, expanded in Fig. 3, where the Nb atoms fall nearly over a Cu atom at the interface. As a result, the bond between the Nb and Cu atom is highly strained prior to relaxation of the interface, causing the two atoms to be deflected from the interface upon relaxation. Previous investigations [2] have identified these sites as intersections between interface dislocations. Therefore, in what follows, they will be referred to as MDIs.

The labels He_{In} and He'_{In} define the first and second most stable sites for a He atom and V_{In} indicates the most stable position for a vacancy. For both metals, the energy is lower when we remove a metal atom that is approximately aligned with another one at the opposite side of the interface. This result may be understood in terms of strain reduction. A detailed explanation, based on MD simulations, has been previously given [26]. When a vacancy is created at a noncoincident area in the interface, the attraction established between the vacancy and the atoms of the opposite surface produces an increase of the corrugation in the terminal plane of the neighboring metal. For example, when the Nb atom labeled Nb_n in Fig. 3 is removed, the corrugation in the Cu surface grows to 0.63 (0.58 in the initial interface). On the other hand, the MDI region is already highly corrugated even before a defect is introduced because the nearly coincident atoms of the neighboring metal layers found there are pushed in opposite directions to reduce the atomic repulsion. Then, if one of these atoms is removed, the corrugation decreases, resulting in a lower energy cost to create defects at the MDI areas than elsewhere in the interface.

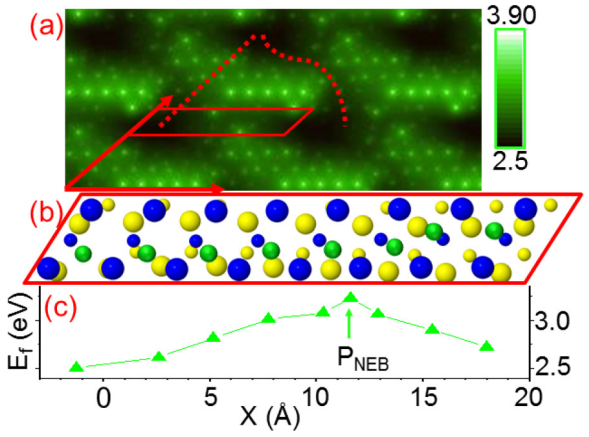

FIG. 4. (Color online) (a) Energetic map obtained from inserting one He atom in one of the 90 Cu-hollow sites of the simulated unit cell, indicated by the red arrows. The map is repeated for several surrounding cells. The red-dotted lines show two alternative paths for He migration. (b) The sphere model inside the red rectangle of Fig. 2. The green spheres represent the most stable sites found for each Cu-1 × 1 unit cell starting from the pair of (hcp or fcc) hollow sites. (c) The formation energies at each He position are presented. The point obtained by means of a NEB simulation between the two highest energy points is indicated.

The situation is more complicated in the case of He atoms. Our results show that He finds enough free space to be accommodated at the empty hollows aligned in the MDIs. The hollow sites at the surfaces correspond to the tetrahedral positions in the metallic bulk, being in both cases the most stable locations for He interstitials. In these points, He interstitials increase the initial corrugation in the interface. On the other hand, for He atoms out of the MDI areas, the hollow site on one side falls near an atom of the opposite metal. This nonalignment may be responsible for the higher energy of the interstitial. Consequently, the combination of both effects (the interface deformation and the alignment of the hollow sites) seems to favor the MDI areas as the lowest energy He interstitial sites.

We have constructed a complete map of He interstitial energies by inserting isolated He atoms in 90 different sites at the interface, which correspond to the different (hcp or fcc) hollow positions in Cu covering the whole interface at nearly equidistant points. In Fig. 4(a) the resulting energetic map obtained for one simulated unit cell is repeated for several surrounding cells to exhibit the periodic pattern of formation energies. Two arrows indicating the interfacial lattice vectors (the same vectors previously shown in Fig. 2) have been included for a better orientation. The most (least) stable sites correspond to the dark (bright) areas. The map shows the great energy cost, of more than 1 eV, for the He atom to move through most of the directions. We have focused our attention on the area inside the red parallelogram [Fig. 4(b)], which can be observed in the complete interface of Fig. 2. The MDI area is located at the left side of the sphere model. The green triangles in Fig. 4(c) represent the formation energy of one He atom (green sphere) placed in the different positions shown in the model in Fig. 4(b). They correspond to the most stable cases obtained for each 1 × 1 Cu unit cell. Interestingly, in

all these cases the He atoms relax to positions closer to the Nb layer and quite close to the tetrahedral sites of a perfect Nb bulk, showing the higher affinity for Nb of the He atoms. The most stable position at the interface presents a formation energy of 2.50 eV, 0.57 eV lower than the least stable one. The red-dotted lines in Fig. 4(a) indicate two alternative paths for He migration along the interface, but both present high energy differences between the most and least stable sites: 0.66 and 0.80 eV, respectively.

Two considerations about the convergence of the calculations should be remarked. First, the formation energy obtained for the most stable site can be compared with the values 3.14 and 3.94 eV found by the authors for the He atoms in tetrahedral positions in the Nb [22] and Cu single crystals [21], respectively. The value for Nb (3.14 eV) has been calculated inside an ideal $5 \times 5 \times 5$ unit cell using 27 k points and the best lattice parameter for VASP (3.316 Å as mentioned before). Using the same conditions but with the strained Nb crystal in our interface model, the resulting formation energy is 3.07 eV, still clearly higher than the lowest value at the interface. On the other hand, the value 0.57 eV has been obtained using 9 k points in the calculation, while for the single Γ point, we obtained 0.55 eV. These results show that our calculations are well converged with respect to the number of k points and that the strain in the Nb side of the interface has only a minor effect on defect formation energies.

The point labeled by P_{NEB} in Fig. 4(c) was found using the NEB technique between the sites of highest formation energy. The energy difference between this point and the most stable one is 0.73 eV. Although for a complete understanding of the migration mechanisms similar NEB calculations should be performed for each pair of points, including some other more complex directions, this value can be considered as a lower bound of the energy barrier for one He atom to move out of an MDI. This energy seems to be much higher than the migration barrier in the perfect bulk metals, namely, 0.125 eV [28] and 0.31 eV for Cu and Nb respectively, suggesting that isolated He atoms will only move at high temperatures in the interface. Consequently, we conclude that isolated He atoms can be trapped at MDIs present at the interface, which is the first step in He cluster nucleation. It is important to notice that if more He atoms manage to reach the interface the situation could change drastically. In such a case, the new He atoms will deform the structure and may reduce energy barriers, easing migration along the interface as observed experimentally [29].

A similar procedure can be followed for one single metallic vacancy. We have performed calculations removing a Cu or Nb atom from all the different positions at the interface. Then, all the energies have been collected in order to create the corresponding energetic maps [Figs. 5(a) and 5(b) for Nb and Cu, respectively]. Again, the dark areas correspond to the most stable vacancy sites at the MDIs, while the brightest points are the less stable ones. The energy differences are 1.19 and 0.92 eV for Cu and Nb, respectively. In agreement with the He case, the most favorable path for vacancy migration is indicated by the red line in each map and the corresponding formation energies are represented in Fig. 5(c).

The line with the circles shows the formation energy for each possible Nb vacancy in that row. The three initial sites from the left have the lowest formation energy values for the

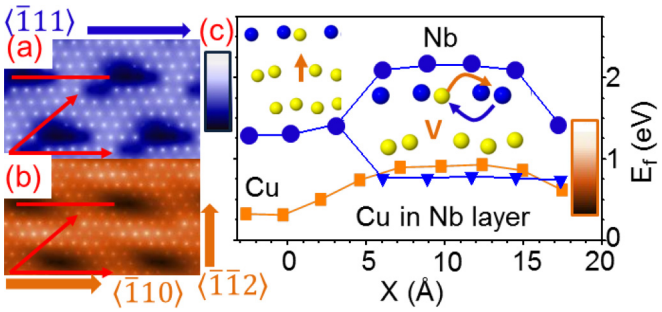

FIG. 5. (Color online) (a) Energetic map of one single Nb vacancy at the Cu/Nb interface. (b) The same for Cu. (c) Formation energies for the vacancies created along the red lines in the maps: blue circles are Nb vacancies, orange squares are Cu vacancies, and blue triangles are Cu vacancies with one Cu atom occupying the empty Nb site, as shown in the inset.

whole MDIs (1.29 eV), much lower than in the perfect bulk (2.66 eV [22] for the ideal lattice parameter for VASP and 2.80 eV for the equivalent lattice derived from the interface). At these sites, as suggested before [26], the Cu atom immediately below the vacancy moves to fill it in, giving rise to an energy gain of 0.84 eV as compared to the less stable cases that lie along a second plateau. A NEB simulation of the migration between two of these latter vacancy sites has been performed and a value of 0.72 eV has been obtained. This value is higher than the migration energy in the bulk, 0.59 eV, as obtained using the same methodology as for W by means of a $4 \times 4 \times 4$ cubic unit cell [28], and in good agreement with experimental data [30]. Adding the calculated migration energy and the difference between both plateaus, the energy cost for the movement of the Nb vacancies out of the MDIs results to be 1.56 eV. Thus, it can be concluded that the Nb vacancies will be stabilized in the MDIs at the interface. Another possible migration process involves the Cu atom embedded in the Nb layer. It could hop from one Nb site to another leaving the vacancy behind in the Cu layer (as schematically indicated in Fig. 5). In this case, the system finds a new plateau of stability that is 0.69 eV lower in energy [see the blue line with triangles in Fig. 5(c)]. Investigating this process would require modeling vacancy-mediated migration of Cu in Nb, which is outside the scope of the current work.

Another alternative situation involves the movement of a Cu vacancy along the red line in Fig. 5(b). The results are shown as the orange squares in Fig. 5(c). Now the lowest formation energy is 0.32 eV in deep contrast with the 1.08 eV obtained in Ref. [21] for the bulk, confirming the great stability of the Cu vacancy at the interface. Additionally, the energy of the system increases by 0.62 eV when the vacancy is created along the red line. A NEB calculation has been performed between the two highest energy sites giving an energy barrier of 1.06 eV, again much higher than the 0.73 eV of the perfect bulk [28]. The total migration energy can be estimated as the difference between the most stable site and the point calculated between the two highest energy sites using the NEB methodology. Then, the total barrier becomes 1.68 eV, which is 0.95 eV higher than the bulk value, suggesting that, as happened with Nb, the Cu vacancy is stabilized at the MDIs.

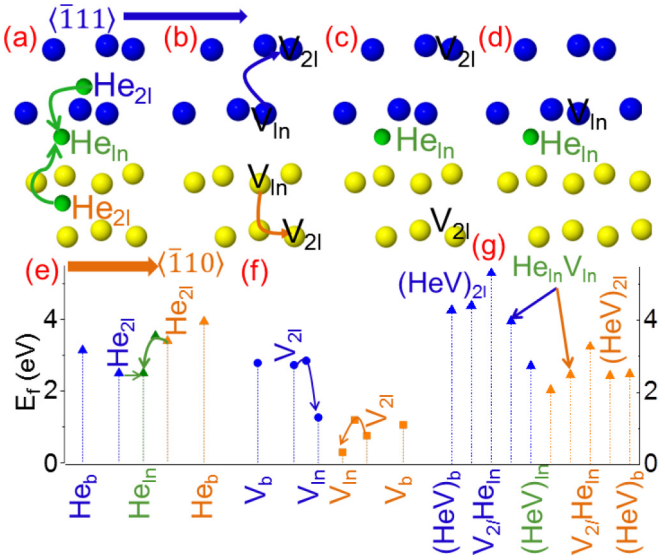

FIG. 6. (Color online) Schematic representation of (a) He migration from the second layer (He_{2l}) to the interface (He_{In}) in each metal, (b) the same for a vacancy (V_{2l} and V_{In}, respectively) in each metal, (c) a vacancy in the second layer and a He atom placed at the most stable site at the interface ($V_{2l}He_{In}$) and (d) the He atom and vacancy separated at the interface ($He_{In}V_{In}$). Blue (yellow) spheres are Nb (Cu) atoms and green spheres are He atoms. In (e), (f), and (g) the formation energies for the different cases in (a), (b), (c), and (d) are represented. Additionally, the formation energies of the following cases can be found: He (He_b) and vacancy (V_b) in the bulk and He occupying a vacancy at the interface, $(HeV)_{In}$, second layer, $(HeV)_{2l}$, and bulk, $(HeV)_b$. Triangles involve He atoms and circles (squares) Nb (Cu) vacancies. Green indicates that the He atom is at the interface, while blue (orange) symbolizes that the defect is in the Nb (Cu) metal.

Due to the intrinsic limitations in the sizes of the supercells used in our simulations, our estimation does not take into account the possibility of delocalized vacancy migration [25].

Interestingly, the fourth point from the left has the same formation energy as the configurations represented by the blue triangles mentioned above. This case is equivalent to first blue triangle but now there is no Cu contamination on the Nb side. All the triangular cases maintained the vacancy in the same Cu site as the fourth orange square. For this reason, we can conclude that the site at which a vacancy is created seems to be more relevant than the kind of atom missed.

In order to understand how the analyzed point defects can reach the interface, we have repeated the simulations with the defects placed at the second layers on both sides of the interface in the vicinity of the MDIs. These situations are schematically depicted in Figs. 6(a) and 6(b). In the following, when both the He atom or the vacancy are in the bulk, at the interface or in the second layer from the interface, they will be denoted as He_b, V_b, He_{In} and V_{In}, He_{2l}, and V_{2l}, respectively. When the He atom is placed in a tetrahedral position between the first and second Nb layers (He_{2l}), it moves directly to the interface showing the great attraction between the two objects. On the other hand, the accommodation of a He atom in a tetrahedral position between the first and second Cu layers requires a formation energy of 3.40 eV, a value that falls in between the interface and bulk numbers explaining the tendency of helium to move to the interface. From this particular site, the calculated migration energy to reach the interface is 0.14 eV, very similar to the bulk value previously mentioned. The Cu vacancy presents a similar behavior: The formation energy at the second layer is 0.78 eV, again in between the bulk and interface values, and the migration energy is 0.44 eV, that is, even lower than in the perfect bulk. Finally, the Nb vacancy at the second layer feels conditions very close to those in the bulk, as its formation energy is very similar (2.75 eV). However, its migration energy (0.12 eV) is much lower than the barrier in the bulk, so diffusion towards the interface is expected in both metals. Both migration processes are schematically represented in Fig. 6(b). All these energies are summarized in graphs 6(e) and 6(f).

TABLE I. Formation energies for different combinations of He atoms in Nb/Cu vacancies: substitutional in the bulk $(HeV)_b$, substitutional or separated at the interface [$(HeV)_{In}$ and $He_{In}V_{In}$], respectively, substitutional in the second layer [$(HeV)_{2l}$], and vacancy in the second layer and He atom at the interface [$V_{2l}He_{In}$].

	E_f (eV)				
	$(HeV)_b$	$(HeV)_{In}$	$He_{In}V_{In}$	$(HeV)_{2l}$	$V_{2l}He_{In}$
Cu	2.52	2.07	2.49	2.46	3.27
Nb	4.27	2.73	3.98	4.39	5.31

So far, we have shown the great energetic gain and high energy cost for migration of the vacancies and He atoms when they are found in interfacial positions. This means that both kinds of defects experience a remarkable trapping effect at the interface. The deep trapping of He atoms inside metallic *n* vacancies (be it vacancy clusters or several single vacancies placed at distant sites) has been firmly established in the literature (see, for instance, Ref. [21], and references therein). Here we denote the He occupying a monovacancy in the bulk as $(HeV)_b$. Thus, it is interesting to compare the affinities of He atoms for the interface and the monovacancy. For that purpose, the previously calculated vacancies have been filled with He atoms at the first and second layers of each metal [denoted as $(HeV)_{In}$ and $(HeV)_{2l}$, respectively], to make a comparison with the helium at the interface. In Fig. 6(c) a schematic of a vacancy in the second layer of each metal and a He atom at the interface is presented (denoted as $V_{2l}He_{In}$). Our results, summarized in Table I and graph 6(g), show that an isolated He atom prefers to occupy the vacancy immediately adjacent to the interface [denoted as $(HeV)_{Int}$] rather than either staying at the interface itself or staying both He and vacancy separated at the interface [denoted as $He_{In}V_{In}$ and represented in Fig. 6(d)]. In fact, there is a great energetic increase when the He atom is at the interface, while the vacancy stays in the second layer ($V_{2l}He_{In}$). This suggests that the He substitutionals will arrive at the interface due to a complex movement together with metal vacancies.

IV. CONCLUSIONS

In conclusion, we have shown the great trapping exerted by the Cu/Nb interface on metallic vacancies and He atoms.

To obtain these conclusions, we performed DFT calculations on a noncoherent Cu/Nb interface. The results presented also contribute to clarifying the diffusive behavior of He atoms in the vicinity of these interfaces. The large mobility of He atoms due to their low migration energies in perfect crystal Cu and Nb explains their facility to reach the interface as observed experimentally. Our calculated migration energies from the second to the first layers show a reduction with respect to the bulk values, thus favoring such a motion. Once the defects find the interface, the isolated He atoms or vacancies stay frozen due to the high energy barrier that should be overcome to move out of the MDIs. Even though the He atoms have lower energy at the interface than in the bulk, they find an even better accommodation inside a metallic vacancy close to the interface, suggesting an enhancement of the trapping effect in this situation.

ACKNOWLEDGMENTS

This work has been funded by the FP7 project RADINTERFACES and the Spanish Ministry of Economy and Competitiveness project NANO-EXTREM, Ref. MAT2012-38541. The authors thankfully acknowledge the computer resources, technical expertise and assistance provided by the Red Española de Supercomputación (RES) project FI-2014-1-0008 and the European PRACE-3IP project (FP7 RI-312763) resource Fionn based in Ireland at ICHEC. M.J.D. acknowledges support from the U.S. Department of Energy, Office of Science, Office of Basic Energy Sciences under Award No. 2008LANL1026 through the Center for Materials at Irradiation and Mechanical Extremes, an Energy Frontier Research Center at Los Alamos National Laboratory.

[1] S. J. Zinkle and J. T. Busby, Structural materials for fission & fusion energy, Mater. Today **12**, 12 (2009).

[2] M. J. Demkowicz, R. G. Hoagland, and J. P. Hirth, Interface structure and radiation damage resistance in Cu-Nb multilayer nanocomposites, Phys. Rev. Lett. **100**, 136102 (2008).

[3] M. J. Demkowicz, A. Misra, and A. Caro, The role of interface structure in controlling high helium concentrations, Curr. Opin. Solid State Mater. Sci. **16**, 101 (2012).

[4] T. Höchbauer, A. Misra, K. Hattar, and R. G. Hoagland, The influence of interfaces on the storage of ion implanted He in multilayered metallic composites, J. Appl. Phys. **98**, 123516 (2005).

[5] A. Misra, M. J. Demkowicz, X. Zhang, and R. G. Hoagland, Radiation damage tolerance of ultra-high strength nanolayered composites, JOM **59**, 62 (2007).

[6] K. Hattar, M. J. Demkowicz, A. Misra, I. M. Robertson, and R. G. Hoagland, Arrest of He bubble growth in Cu–Nb multilayer nanocomposites, Scr. Mater. **58**, 541 (2008).

[7] M. Victoria, S. Dudarev, J. L. Boutard, E. Diegele, R. Lässer, A. Almazouzi, M. J. Caturla, C. C. Fu, J. Källne, L. Malerba, K. Nordlund, M. Perlado, M. Rieth, M. Samaras, R. Schaeublin, B. N. Singh, and F. Willaime, Modelling irradiation effects in fusion materials, Fus. Eng. Des. **82**, 2413 (2007).

[8] A. Kashinath and M. J. Demkowicz, A predictive interatomic potential for He in Cu and Nb, Model. Simul. Mater. Sci. Eng. **19**, 035007 (2011).

[9] A. Y. Dunn, M. G. McPhie, L. Capolungo, E. Martínez, and M. Cherkaoui, Helium bubble formation and retention in Cu-Nb nanocomposites, J. Nucl. Mater. **435**, 141 (2013).

[10] A. Kashinath, A. Misra, and M. J. Demkowicz, Stable storage of Helium in nanoscale platelets at semicoherent interfaces, Phys. Rev. Lett. **110**, 086101 (2013).

[11] A. J. Vattré, N. Abdolrahim, K. Kolluri, and M. J. Demkowicz, Computational design of patterned interfaces using reduced order models, Sci. Rep. **4**, 6231 (2014).

[12] W. Xiao and W. T. Geng, Role of grain boundary and dislocation loop in H blistering in W: A density functional theory assessment, J. Nucl. Mater. **430**, 132 (2012).

[13] W. Körner, P. D. Bristowe, and C. Elsässer, Density functional theory study of stoichiometric and nonstoichiometric ZnO grain boundaries, Phys. Rev. B **84**, 045305 (2011)

[14] L. Huber, J. Rottler, and M. Militzer, Atomistic simulations of the interaction of alloying elements with grain boundaries in Mg, Acta Mater. **80**, 194 (2014).

[15] A. Hunter and I. J. Beyerlein, Stacking fault emission from grain boundaries: Material dependencies and grain size effects, Mater. Sci. Eng., A **600**, 200 (2014).

[16] Y. Mishin, M. Asta, and J. Li, Atomistic modeling of interfaces and their impact on microstructure and properties, Acta Mater. **58**, 1117 (2010).

[17] E. Metsanurk, A. Tamm, A. Caro, A. Aabloo, and M. Klintenberg, First-principles study of point defects at a semicoherent interface, Sci. Rep. **4**, 7567 (2014).

[18] G. Kresse and J. Hafner, *Ab initio* molecular dynamics for liquid metals, Phys. Rev. B **47**, 558(R) (1993); G. Kresse and J. J. Furthmuller, Efficient iterative schemes for ab initio total-energy calculations using a plane-wave basis set, *ibid.* **54**, 11169 (1996); G. Kresse and D. Joubert, From ultrasoft pseudopotentials to the projector augmented-wave method, *ibid.* **59**, 1758 (1999).

[19] P. E. Blöchl, Projector augmented-wave method, Phys. Rev. B **50**, 17953 (1994).

[20] J. P. Perdew, K. Burke, and M. Ernzerhof, Generalized gradient approximation made simple, Phys. Rev. Lett. **77**, 3865 (1996).

[21] C. González, D. Fernández-Pello, M. A. Cerdeira, S. L. Palacios, and R. Iglesias, Helium bubble clustering in copper from first principles, Model. Simul. Mater. Sci. Eng. **22**, 035019 (2014).

[22] C. González, M. A. Cerdeira, S. L. Palacios, and R. Iglesias, Reduction of the repulsive interaction as origin of helium trapping inside a monovacancy in BCC metals (unpublished).

[23] A. M. James and M. P. Lord, *Macmillan's Chemical and Physical Data* (Macmillan, London, UK, 1992).

[24] G. V. Kjurdumov and G. Sachs, Über den Mechanismus der Stahlhärtung, Z. Phys. **64**, 325 (1930).

[25] K. Kolluri and M. J. Demkowicz, Dislocation mechanism of interface point defect migration, Phys. Rev. B **82**, 193404 (2010).

[26] M. J. Demkowicz, J. Wang, and R. G. Hoagland, in *Dislocation in Solids Vol. 14: A Tribute to F. R. N. Nabarro*, edited by J. P. Hirth (Elsevier B. V., Amsterdam, 2008), p. 141.

[27] H. Jonsson, G. Mills, and K. W. Jacobsen, in *Classical and Quantum Dynamics in Condensed Phase Simulations*, edited by B. J. Berne, G. Ciccotti, and D. F. Coker (World Scientific, Singapore, 1998), p. 385.

[28] C. González and R. Iglesias, Migration mechanisms of helium in copper and tungsten, J. Mater. Sci. **49**, 8127 (2014).

[29] M. J. Demkowicz, Y. Q. Wang, R. G. Hoagland, and O. Anderoglu, Mechanisms of He escape during implantation in CuNb multilayer composites, Nucl. Instrum. Methods Phys. Res., Sect. B **261**, 524 (2007).

[30] H. Schultz, in *Atomic Defects in Metals*, edited by H. Ullmaier, Landolt-Bornstein, New Series III/25 (Springer, New York, 1991).